TECHNICAL MEMORANDUMS

NATIONAL ADVISORY COMMITTEE FOR AERONAUTICS

TM No. 739

EXPERIMENTS WITH PLANING SURFACES

By W. Sottorf

Werft-Reederei-Hafen

October 1, 1932; February 15, and March 1, 1933

Washington
March 1934

NATIONAL ADVISORY COMMITTEE FOR AERONAUTICS

TECHNICAL MEMORANDUM NO. 739

EXPERIMENTS WITH PLANING SURFACES*

By W. Sottorf

A previous report (reference 1) discusses the experimental program of a systematic exploration of all questions connected with the planing problem as well as the first fundamental results of the investigation of a flat planing surface. The present report is limited to the conversion of the model test data to full scale.

According to Froude's method, the results of model experiments on ships are converted conformably to the formula

$$W = (w - c_m f' \frac{\rho}{2} v^2) \lambda^3 + c_s F' \frac{\rho}{2} V^2$$

where W is the resistance of the full-sized craft

w, total model resistance

$c_m f' \frac{\rho}{2} v^2$, frictional resistance of model

$c_s F' \frac{\rho}{2} V^2$, frictional resistance of full size

in which

c_m is the coefficient of friction of the model

c_s, coefficient of friction of full size

f', wetted surface of model

F', wetted surface of full size

---

*"Versuche mit Gleitflächen." Werft-Reederei-Hafen, October 1, 1932, pp. 285-290; February 15, 1933, pp. 43-47; and March 1, 1933, pp. 61-66.

v, speed of model

V, speed of full size

$\rho = \frac{\gamma}{g}$, density of water

λ, scale

The frictional resistance is subtracted from the measured model resistance, and the residual resistance, containing form and eddy resistance, is multiplied by the third power of the scale, so as to give the form and eddy resistance for full size. Lastly, the frictional resistance for full size is added.

The calculation of the frictional resistance of both model and full size is effected with friction coefficients obtained from towing flat, almost displacementless surfaces, in which it is assumed that the boundary layer condition affecting the coefficient is the same for both ship and model. The wetted surface f' is developed for the model below the water line at rest and is assumed equal to the wetted surface of the model under way. A further assumption is that the local increases and decreases of speed that appear on the ship as the effects of displacement flow and the wave system, are to be disregarded relative to the model and ship speed used in the formula. Searching analyses of trial runs have shown that the accuracy of conversion with ship-model experiments averaged ± 2 percent of the power and ± 1 percent of the revolutions, thus demonstrating that the simplifying assumptions made in the conversion formula are permissible.

The conversion of the towing test results of planing water craft, that is, especially of planing boats, airplane floats and hulls to full size, is not possible with the same method because:

1) The wetted surface changes with the speed and with the angle of trim;

2) The mean speed of the water on a planing surface differs substantially from the towing speed, as confirmed by the pressure measurements of reference 1;

3) At smaller scales, the friction coefficients at equal Reynolds Numbers may assume different values, depending upon whether the boundary layer is laminar or turbulent, or turbulent after laminar approach.

SCALE TESTS WITH PLANING SURFACES

In order to clear up these points the planing surface tests were carried through to point 5 of the test program. It was shown (reference 1) that the total resistance of a flat bottom in pure planing condition, where top as well as side edges are free of water and hence only under atmospheric pressure, is

$$W = A \tan \alpha + \frac{T}{\cos \alpha}$$

The horizontal component of the frictional resistance then is

$$W_R = W - A \tan \alpha$$

and the frictional resistance parallel to the surface is

$$T = W_R \cos \alpha$$

so the coefficient of frictional resistance is

$$C_f = \frac{T}{F' \frac{\rho}{2} v_m^2}$$

Here the wetted surface is introduced as a measured quantity and for the determination of the mean speed v_m of the water over the planing surface, the reduction in speed $v_u = f(\alpha)$ in reference 1 is resorted to.

Starting with run No. 42-52 (reference 1, page 12) with the flat planing surface A of $b_1 = 0.3$ m beam, at 6 m/s speed and 18 kg load, the investigation is continued conformably to the Froude law on five other similar planing surfaces.

---

m × 39.37 = in. m/s × 3.28083 = ft./sec. kg × 2.20462 = lb.

For a similar planing surface of beam b_2 the scale is then $\lambda = \frac{b_2}{b_1}$, the corresponding speed $v^2 = \sqrt{\lambda}\, v_1$ and the load $A_2 = \lambda^3 A_1$. The test schedule for the six planing surfaces tested, is as follows:

Planing surface	b m	v m/s	A kg
1	0.600	8.48	144.000
2(A)	0.300	6.00	18.000
3	0.225	5.20	7.600
4	0.150	4.24	2.250
5	0.100	3.46	0.660
6	0.075	3.00	0.281

The different surfaces were tested at constant load and speed and variable moment, and in each case the resistance, trim, and wetted length were measured.

The test set-up for the two larger models is, in principle, the same as described in reference 1. On the smaller models the dynamometer and the trim rods were disconnected for the sake of accuracy, and the measurements are made as pendulum measurements, using a very flexible spring. The planing surfaces are located behind a wind screen, thus avoiding any air-speed effect.

RESULTS

Tabulation of Test Data

Run No.	α	$\frac{F'}{b^2}$	$\epsilon = \frac{W}{A}$	$\frac{M^*}{A\,b}$	R	c_f
	Surface 1: b = 0.6 m, A = 144 kg, v = 8.48 m/s					
	deg. min.					
1	4 46	2.318	0.1403	1.430	8.75×10^6	0.00279
2	5 8	1.816	0.1403	1.373	7.67×10^6	0.00287
3	5 34	1.733	0.1410	1.194	6.62×10^6	0.00285
4	5 34	1.766	0.1403	1.122	6.62×10^6	0.00280
5	6 5	1.360	0.1410	1.000	5.45×10^6	0.00285
6	6 52	1.167	0.1438	-	-	-

*Axis of moment is after edge of planing surface.

Tabulation of Test Data (Cont.)

Run No.	α	$\frac{F'}{b^2}$	$\epsilon = \frac{W}{A}$	$\frac{M^*}{A\,b}$	R	c_f
	Surface 2: b = 0.3 m, A = 18 kg, v = 6 m/s					
	deg. min.					
7	2 36	4.670	0.1845	2.660	6.41×10^6	0.00327
8	3 47	3.050	0.1600	2.145	4.22×10^6	0.00333
9	3 58	2.918	0.1566	2.060	3.98×10^6	0.00333
10	4 10	2.700	0.1567	2.015	3.68×10^6	0.00348
11	4 15	2.600	0.1540	1.840	3.56×10^6	0.00339
12	4 26	2.395	0.1508	1.760	3.26×10^6	0.00343
13	5 8	1.935	0.1442	1.171	2.63×10^6	0.00317
14	5 12	1.885	0.1470	1.416	2.545×10^6	0.00338
15	5 31	1.717	0.1460	1.308	2.28×10^6	0.00332
16	5 40	1.634	0.1460	1.215	2.16×10^6	0.00339
17	6 53	1.060	0.1505	0.836	1.41×10^6	0.00331
18	7	1.000	0.1505	0.765	1.315×10^6	0.00334
19	7 54	0.783	0.1595	0.570	1.000×10^6	0.00331
20	8 58	0.606	0.1695	0.450	-	-
21	9 34	0.544	0.1760	0.405	-	-
	Surface 3: b = 0.225 m, A = 7.6 kg, v = 5.2 m/s					
22	3 27	3.450	0.1710	2.313	3.07×10^6	0.00355
23	4	2.850	0.1622	1.995	2.52×10^6	0.00362
24	4 57	2.010	0.1520	1.355	1.762×10^6	0.00368
25	5 37	1.560	0.1486	1.090	1.360×10^6	0.00372
26	6 41	1.110	0.1520	0.828	0.955×10^6	0.00374
26a	6 40	1.110	0.1520	0.828	0.955×10^6	0.00374 8% roughened
26b	6 38	1.125	0.1560	0.828	0.955×10^6	0.00420 16% roughened
26c	6 38	1.145	0.1683	0.828	0.955×10^6	0.00541 32% roughened
27	7 48	0.822	0.1613	0.580	0.690×10^6	0.00371
	Surface 4: b = 0.15 m, A = 2.25 kg, v = 4.24 m/s					
28	2 57	3.500	0.2000	2.380	-	-
29	4 19	2.467	0.1720	1.817	1.19×10^6	0.00439
30	4 43	2.053	0.1645	1.534	9.86×10^5	0.00452
31	5 30	1.698	0.1623	1.288	8.10×10^5	0.00445
32	6 12	1.350	0.1578	0.993	6.37×10^5	0.00427
33	8	0.787	0.1662	0.504	3.57×10^5	0.00411

Tabulation of Test Data (Cont.)

Run No.	α	$\frac{F'}{b^2}$	$\epsilon = \frac{W}{A}$	$\frac{M^*}{A\ b}$	R	c_f
	Surface 5: b = 0.1 m, A = 0.660 kg, v = 3.46 m/s					
	deg. min.					
34	2 53	3.900	0.2820	2.135	-	-
35	4 25	2.600	0.2258	1.755	6.82×10^5	0.00634
36	5 4	2.150	0.2000	1.565	5.59×10^5	0.00584
37	5 29	1.820	0.1880	1.255	4.71×10^5	0.00575
38	5 56	1.500	0.1788	0.952	3.97×10^5	0.00574
39	7 8	1.000	0.1726	0.640	2.51×10^5	0.00573
40	8	0.750	0.1803	0.444	1.85×10^5	0.00661
	Surface 6: b = 0.075 m, A = 0.281 kg, v = 3 m/s					
41	2 59	3.860	0.3220	2.300	6.63×10^5	0.00768
42	3 42	3.200	0.2825	2.155	5.42×10^5	0.00757
43	4 50	2.200	0.2360	1.450	3.82×10^5	0.00760
44	6	1.535	0.2110	1.040	2.56×10^5	0.00806
45	7 9	1.000	0.1850	0.480	1.76×10^5	0.00675
46	8 6	0.868	0.1911	0.414	1.40×10^5	0.00718
47	9 32	0.667	0.2100	0.283	1.03×10^5	0.00872

Mean reduction in speed over the planing surface $v_u = v - v_m$.

α =	2°	4°	6°	8°	10°
v_u =	0.4%	1.3%	3.4%	7.2%	13.2%

Figure 1 shows planing number $\epsilon = \frac{W}{A}$ versus trim angle α for all investigated surfaces. It is apparent that the smaller the scale the less favorable ϵ becomes. It is particularly notable that the change from the conditions in which the edges of the planing surfaces are wet. to that of pure planing occurs at very small trim angles for the larger scales, while at the small scales it occurs at larger angles the smaller the surface as seen from the boundary curve. This demonstrates the dissimilarity of flow pattern when the scale is too small.

Figure 2 gives the friction coefficients $c_f = \frac{W_R \cos \alpha}{F' \frac{\rho}{2} v_m^2}$ versus the Reynolds Number $R = \frac{v_m l'}{\nu}$. The curves I, II, and III show the experimental points that

have been obtained in friction tests by the formation of laminar, turbulent, and turbulent boundary layer with laminar approach. According to the tests in this range, the alternate creation of different conditions of the boundary layer should result in considerable variation in the coefficients. In contrast, it can be stated as a most important result of these tests, that the scatter of the coefficients corresponding to a single surface is very small.

It should be noted that the whole scatter of the points applies to the frictional resistance W_R of the formula, as a result of which, at higher trim angles with a correspondingly smaller proportion of W_R, there must result an apparently greater scatter. Furthermore, the wetted length l' and correspondingly the wetted surface F', enter as measured quantities as a result of which the scatter for small wetted lengths increases because of errors of reading of small absolute magnitude.

The individual test points were determined partly in entirely calm water, as at the beginning of the runs and after stops, and partly in slightly rough water. Consequently the small scatter of the test points attests to the existence of only a single temporarily stable form of the boundary layer. The values for any one planing surface are approximately constant. The coefficients increase as the mean Reynolds Number decreases. At equal Reynolds Number the coefficients for the different surfaces vary, which is explained by the fact that the trim angles of the surfaces and as a result, the mean pressures and the pressure rises at the leading edges are dissimilar, with consequent effect on the boundary layer. The different roughness of the planing surfaces presents a possibility of influencing the coefficients. To ascertain whether the different degrees of roughness at the leading edge of the wetted surface may influence the coefficients which lie below the curve of the turbulent friction, the roughened surface No. 3, for comparison with run 26, in which a wetted length of 250 mm was observed, was further roughened over its whole width for 20 mm, that is, between 230 and 250 mm of its length, and then, consecutively, for 40 mm and for 80 mm. The result was that the first, 8 percent roughness, produced no increase in resistance, the second with 16 percent roughening, a 12.3 percent increase, and the third, with 32 percent roughening, a 31 percent increase in resistance. This shows that the boundary layer condition underwent no change with 8 percent roughening,

---

mm × .03937 = in.

and that an increase in coefficient as roughness effect occurs only with extensive roughness.

The surface coefficient F'/b^2 and moment coefficient M/Ab are plotted against α in figure 3. No legitimate deviation from a mean curve being established for both factors, it may be stated that within the range investigated, similarity of wetted surfaces, similarity of moments, and hence similarity of pressure distribution does exist.

SCALE TESTS WITH FLOATS

The investigations thus far are applicable to one load case at a speed where the pure planing condition has developed. But in float experiments the region of the hump resistance wherein this planing condition is as yet not fully developed, is also of great importance. So, in order to ascertain the effect of the scale on the hump resistance, a series of tests was made with floats of different scales. The first test was a towing test of a single full-sized float type HS1H at a load of 1,200 kg - equivalent to half the gross weight - that was carried to the maximum speed that could be reached free to trim in the experimental tank 9.5 m/s. The load on the float was reduced according to the formula

$$E = G \frac{V^2}{V_s^2}$$

where V_s is the get-away speed = 23.33 m/s. The load was not reduced to correspond with the change in trim as it is unnecessary in a study of scale effect. The center of gravity position in height and length, as well as the point of application of the towing pull was fixed. The resistance and trim were measured and at one speed the shape of the spray in a plane at right angles to the float was also determined. Other scales selected were $\lambda = 3, 6, 9$, and 12.

Each model float was tested under identical conditions conformably to the Froude model law. These test series give the effect of the scale on resistance, trim, and shape of spray at the same moment.

Other test curves were obtained in the region of the hump resistance by bringing the models to the same trim condition by altering the moment, as the full-sized float.

These experiments give the effect of the scale on resistance and moment at the same trim; that is, the actual scale effect resulting from the change in friction coefficients if it can be assumed that at the same angle of trim not only the planing surfaces under pressure but also the areas of the afterbody wetted by the spray, are similar.

RESULTS

Figures 4 and 5 give resistance and trim angles of the full-scale float and also of the model floats, for which $W = w\lambda^3$ has been desired. For instrumental reasons, the first full-sized float test could not be run above 8.75 m/s; only in the next test with a different moment could the maximum be clearly determined.

Figure 6 shows the manner in which the percentage of increase in resistance varies with λ at maximum resistance when m = constant and when α = constant:

λ	m = constant	α = constant
3	3.5 percent	8.5 percent
6	6.0 "	10.5 "
9	10.5 "	17.0 "
12	21.5 "	25.0 "

The angles of trim prior to reaching the hump resistance are the same. With the beginning of the planing condition, a shift of the trim angle occurs which, for this series of tests amounts to about 1° between each of the scales selected. The increase in resistance for a single surface is practically constant, the percentage of increase therefore rises as the speed. The change from $\lambda = 9$ to $\lambda = 12$ is accompanied by a marked increase in resistance.

The effect of this increase on the get-away time depends on the magnitude of the propeller thrust. The get-away time is

$$t = \frac{G}{g}\int_0^{V_s} \frac{1}{S - W}\,dv$$

where G is the airplane weight

S, propeller thrust

W, total resistance = water + air resistance

V_S, get-away speed

If the resistance curve of the full-sized float is extrapolated from the test curves of the different models, the increase in the get-away time would be

At	$\lambda=3$	$\lambda=6$	$\lambda=9$	$\lambda=12$
20% excess thrust at the hump	3.8%	10.9%	26.0%	146.0%
40% " " " " "	3.0%	6.0%	12.0%	34.0%

EFFECT OF SCALE ON SPRAY FORMATION

The form of the sheet of the spray in a transverse plane 0.5 m forward of the step was recorded by means of measuring rods for the full-sized float at a speed of 8.75 m/s and for the models at corresponding speeds and corresponding locations. The results converted to full size are shown in figure 7. Bearing in mind that no sharp transition from the spray-contacted space to the free space occurs, which might result in a certain scatter during the measurement, it will be noted that there is clearly a reduction of the relative height of spray as the model becomes smaller, the drops formed being of the same size because of the same surface tension of the water at all scales. Consequently, if appendages of the model lie in the spray, such as wing-tip floats, stub-wing stabilizers, or landing gear of amphibians, they are washed dissimilarly by the spray at different scales. The difference in spray formation is readily apparent in the comparative runs of the models at $\lambda = 3$ and $\lambda = 12$ (figs. 8 and 9).

SELECTION OF SCALE

Because of the effect of frictional resistance, the influence of the scale is dependent on the magnitude of wetted surfaces. These in turn are, with equal load, de-

pendent on the angle of dead rise and the shape of the float aft of the step. Consequently, the data obtained with one specific type of float can only serve as a reference for the limitation of the scale.

The first stipulation is that the flow conditions of model and full size shall be similar. Referring the width of the float of 0.957 m as full size to the planing surfaces, gives surface No. 5 a scale of $\lambda = 9.57$. At mean trim surface No. 5 does not produce the pure planing condition as at the larger scales. Thus the planing experiments show that, beginning at $\lambda \simeq 9$ the flow pattern is partly dissimilar, for which reason no further reduction in scale is advisable, a fact confirmed by the marked increase in resistance between $\lambda = 9$ and $\lambda = 12$.

If, in view of the frictional differences, it becomes impossible to convert the model data to full size as illustrated, then the second requirement is, that even when the scale effect is disregarded, results shall be obtained which vary only within the usual limits of accuracy in model tests from the true figures. The float experiments have shown that with $\lambda = 4$, the maximum resistance is exceeded by less than 5 percent, the trim angle differs only by about 1°, and the get-away time is given only 4 to 5 percent too high at 20 to 40 percent excess of thrust. Also, the spray with this scale is practically the same as for full size. It is therefore advisable to investigate floats of this order of magnitude at $\lambda = 4$.

For larger aircraft, such as flying boats, it is not necessary to hold to this scale, for the chart of figure 2 clearly shows that with further increase in the dimensions, the frictional coefficients do not become particularly smaller. From the point of view of load, the float of average size may be considered a model of a flying boat without producing a notable change in the friction coefficient within this range of enlargement. If, for instance, one is dealing with a gross weight of 9,600 kg, then at a gross weight of 1,200 kg of the float the scale is $\lambda' = \sqrt[3]{\frac{9600}{1200}} = 2$. A model of the flying boat at a scale of $\lambda \lambda' = 4 \times 2 = 8$ will therefore give almost the same accuracy of conversion as the model of the float at a scale of $\lambda = 4$. Naturally, a larger scale is to be preferred, about $\lambda = 6$, if the test equipment permits the use of such large models. By the construction of its new tank

for towing at high speeds, which was described in W.R.H. for 1931, No. 11, the Hamburgische Schiffbau Versuchsanstalt has provided the equipment for using these large models.

On the basis of tests of different similar planing surfaces and different similar floats the effect of the scale of the model on the conversion of the results to full size is discussed for the case where the formula, applied to the conversion of tests of ship models, which takes account of the different values of the friction coefficients for model and full size, cannot be used.

EFFECT OF V-BOTTOM

V-bottoms are used in seaplane design in order to reduce the shocks on the bottom during take-off and landing in a seaway, which may become several times greater than the gross weight of the airplane. We refer here to Wagner's report (reference 2) and Pabst's report (reference 3). Figure 10, which shows the reduction of landing impact with increasing angle dead rise compared to the flat bottom, was taken from Pabst's article. However, there is a limit to the angle of dead rise because the planing resistance is a minimum when the bottom is flat and rises as the dead rise becomes greater. This means, providing there is nothing else to prevent the take-off, a substantially longer take-off run, and the opinions of the designers relative to the requirements in a seaway are still very much divided as to whether a quicker get-away with a flat or slightly V'd bottom or a longer take-off with pronounced V-bottom is more advantageous.

Qualitatively an increase in resistance is obtained with increasing dead rise, according to the following analysis: Consider that part of a flat-bottom float which, relative to the direction of motion, is straight; in a frictionless fluid the resistance is $W = A \tan \alpha$ if the load A is given. On a V-bottom (fig. 11c) the normal pressure on each side is $N/2$, and its vertical component $A/2$, where A is the total load carried by the two sides. The loss components $D/2$ are canceled. The resistance is the sum of the components in the direction of motion: $W/2 = A/2 \tan \alpha$, that is, $W = A \tan \alpha$. Accordingly, in a frictionless fluid the resistance of flat- and V-bottoms is the same.

In a viscous fluid (fig. 11b) the friction T becomes additive. Then $W = A \tan \alpha + T/\cos \alpha$. T is approximately proportional to the wetted surface F', which increases with increase of the sum of the normal forces exerted on either side of the bottom to generate the lift A. N and consequently F' and T are minimum for the plane surface where N falls in the median plane, whereas N and consequently F' and T increase steadily with the increasing dead rise. Accordingly, the total resistance of a V-bottom increases with the dead rise. The percent decrease in performance due to the dead rise is greatest at small angles of trim where the proportion of the frictional to the total resistance is greatest, as seen from the total resistance distribution (fig. 12, reference 1).

Another disadvantage of V-bottoms is the much greater spray formation at the sides which, through impact on appendages may multiply the resistance and endanger the propeller and the control surfaces. This explains the attempt to keep the spray at a minimum by special design of the edges of the planing bottom. The purpose of the investigation of the four straight V-bottom (flat fore and aft) planing surfaces Nos. 7 to 10, in contrast with the flat planing surface A, is to establish the effect of the dead rise on the resistance, moment, wetted surface, spray formation, and pressure distribution. The width A of each planing surface is 0.3 m, and they have been tested at a speed of 6 m/s and a load of 18 kg, in comparison with the runs Nos. 42 to 52 with the planing surface A described in reference 1. The pressure distribution and the spray formation have been determined at identical speed and load for $\alpha = 4^\circ$, 6°, and 8°. (See fig. 12.)

MEASUREMENT OF SPRAY FORMATION AND PRESSURE DISTRIBUTION

The spray contours at the side of the planing surface and the hollow wake or trough aft of it, were measured in a number of longitudinal and lateral planes by means of measuring needles which are self-locking under spring pressure (as shown in fig. 13). The plotted curves are the upper boundary of the sheet of spray. Isolated sprays that leave the main body are disregarded. The power of the spray which can vary within the contours, can be gaged from the appended photographs.

The spray is formed on the parts of the outside edge

of the planing surface where a large pressure drop occurs. Consequently, for a thorough analysis it is important to be able to draw on records of pressure distribution across the planing bottom. A detailed account of the test procedure and scope for the flat planing surface A is given in reference 1. There, by assuming that the deviation of the streamlines beneath the planing surface from the direction of motion was unimportant, the speed decrease under the planing surface could be defined on the basis of the pressure distribution and introduced as a factor in the computation of the frictional resistance. But this assumption is not presumable with V-bottom surfaces. Consequently, in the estimation of the resistances of different V-bottoms only a resistance change parallel to the change of the wetted surface can be determined. However, after the division of the resistance of (longitudinally straight) planing surfaces at $W_{tot} = A \tan \alpha + T/\cos \alpha$ is confirmed by the results of the flat planing surface A, the use of the pressure distribution across the V surface for computing the friction is no longer necessary.

Each planing surface was provided with about 90 pressure orifices arranged in three longitudinal rows and a number of transverse rows. Figure 14 shows one orifice. The discharge orifice diameter was 2 mm and on three surfaces 1 mm for check testing. The glass tubes above the sta stations were mounted on a support. For the test the planing surface was fixed at the trim angle established in the resistance measurements. When the water is calm, the water pressure can be indicated by marking on the glass. To detect any mutual interference between successive test orifices, several test runs were made in which only one orifice was kept open; the others were closed with Plastiline but no noticeable differences could be detected. The check tests with the 1 mm orifice diameter revealed as a result of the greater throttling of the entering water, a smaller fluctuation in the water column without, however, affecting the average. It required on the average, three test runs for each trim angle, so that minor speed discrepancies were inevitable. Consequently, the experiments cannot claim to give the pressures with an accuracy of more than about ±5 percent.

The recorded maximum pressures for all surfaces are substantially below the dynamic pressure which at $v = 6$ m/s, is 0.1835 kg/cm^2 or 1835 mm water pressure. Even though the range in which the dynamic pressure is measured

is very narrow, the 800 mm long tubes must have proved too short at times for the much closer-spaced orifices in the forward pressure zone, as these tubes change their position relative to the pressure zone during a test run even with the least movement of the water. Since this was not the case, it may be assumed that the dynamic pressure does not occur on the surface.

RESULTS

Planing Surfaces A and 7 to 10

Run No.	α	$\frac{F'}{b^2}$	$\epsilon = \frac{W}{A}$	$\frac{M^*}{A\ b}$	$\frac{l_p}{l_F}$
	Surface A: b = 0.3 m; A = 18 kg; v = 6 m/s				
	deg. min.				
42	2 36	4.670	0.1845	2.657	0.633
43	3 47	3.050	0.1600	2.145	0.697
44	4 10	2.701	0.1567	2.013	0.704
45	4 10	2.602	0.1538	1.839	0.729
46	5 8	1.935	0.1442	1.172	0.748
47	5 31	1.717	0.1461	1.308	0.752
48	5 40	1.635	0.1461	1.215	0.760
49	6 53	1.062	0.1505	0.836	0.767
50	7 54	0.784	0.1595	0.570	0.785
51	8 58	0.606	0.1669	0.450	0.740
52	9 34	0.545	0.1761	0.404	0.733
	Surface 7: b = 0.3 m; A = 18 kg; v = 6 m/s				
1	3 42	3.570	0.1710	2.255	
2	4 46	2.390	0.1583	1.670	
3	5 20	1.968	0.1555	1.409	
4	5 51	1.678	0.1550	1.215	
5	6 46	1.272	0.1594	0.938	
6	8 7	0.902	0.1661	0.662	
7	9 10	0.712	0.1761	0.528	
8	10 4	0.615	0.1861	0.458	
	Surface 8: b = 0.3 m; A = 18 kg; v = 6 m/s				
9	3 34	4.180	0.1945	2.280	
10	4 25	3.032	0.1805	1.945	
11	5 25	2.300	0.1711	1.570	
12	6 3	1.832	0.1667	1.274	
13	6 34	-	0.1673	1.128	
14	7 44	1.163	0.1700	0.845	
15	8 23	0.093	0.1745	0.705	
16	9 61	0.866	0.1816	0.568	

*Axis of moments is after edge of keel line.

Planing Surfaces A and 7 to 10 (cont.)

Run No.	α	$\frac{F'}{b^2}$	$\epsilon = \frac{W}{A}$	$\frac{M^*}{Ab}$
	Surface 9: b = 0.3 m; A = 18 kg; v = 6 m/s			
	deg. min.			
17	3 55	4.370	0.2083	2.203
18	4 46	3.443	0.1960	1.900
19	5 34	2.730	0.1900	1.607
20	6 46	2.038	0.1922	1.316
21	7 12	1.853	0.1910	1.179
22	7 37	-	0.1910	1.107
23	8 15	1.479	0.1933	0.968
24	8 40	1.342	0.1944	0.890
25	9 17	1.245	0.1955	0.832
26	9 47	-	0.1950	0.765
27	10 00	1.155	0.1972	0.762
	Surface 10: b = 0.3 m; A = 18 kg; v = 6 m/s			
28	2 55	6.600	0.2345	2.753
29	3 15	6.245	0.2368	2.548
30	4 10	5.328	0.2423	2.160
31	4 10	5.328	0.2434	2.160
32	6 -	3.790	0.2423	1.675
33	7 50	3.368	0.2467	1.440
34	8 15	3.145	0.2489	1.258
35	10 5	2.225	0.2572	1.107

The plot (fig. 15) shows the angle of trim α versus planing number $\epsilon = \frac{W}{A}$, moment coefficient $c_M = \frac{M}{A\,b}$ and surface factor $c_F = \frac{F'}{b^2}$ of planing surfaces numbers 7 to 10 and flat surface A. Tan α is the common asymptotical limiting value of the ϵ curves. In accordance with the theoretical analysis, the result shows an increase in resistance rising steadily with increasing angle of dead rise as the wetted surface increases. The harmful effect of the angle of dead rise diminishes as the trim angle increases. because the proportion of frictional resistance to total resistance decreases. Figure 16 shows the percent increase of the minimum resistance as well as the resistances at $\alpha = 4^\circ$ and 10° compared to that of the flat planing surface as they vary with the bottom angle β. As the load increases, ϵ becomes worse. (See fig. 10, reference 1.) Then the effect of the dead rise will be more appreci-

able at high angles of trim, whereas it will be less at low loads. Figure 17 gives the mean specific pressure $p_m = \frac{A}{F!}$ in fractions of the dynamic pressure $q = \frac{\rho}{2} v^2$ against β at $\alpha = 4^\circ$, 6°, and 8°. The plot also shows the static draft V corresponding to the momentary position of the planing surface in planing condition expressed in fractions of draft V necessary for buoyancy A in rest position. It is seen that p_m/q drops sharply as the angle of V increases, whereas V/V_A increases.

FORMATION OF SPRAY

Planing surface A (fig. 19) shows a portion of the spray profiles measured at $\alpha = 4^\circ$, 6°, and 8°, a photograph at $\alpha = 6^\circ$, and the pressure distribution for $\alpha = 6^\circ$.*

As concerns the water trough aft of the planing surface: because of the small pressure drop the water leaves in the direction of the planing surface and in the plane of symmetry reaches about the same depth below the water level for all angles of trim, although always deeper than the deepest point of the planing surface. The surface of the water in the long trough is almost smooth. The trough is bounded by the two waves that proceed from the sides and meet aft in the plane of symmetry. At their meeting, the water rises in a jet forming a roach. This roach moves rearward with increasing angle of trim as well as with increasing beam of the planing surface. With increasing speed and simultaneous decrease of the load on the planing surface, a case analogous to the take-off cycle, the roach moves in toward the step. This means that in take-off shortly before the get-away the afterbody may be again wetted by spray from the roach, with which a considerable increase in resistance is entailed.

Because of the marked pressure drop, the lateral spray rises steeply at the side edge and has, at the rear edge of the planing surface, which corresponds to the location

---

*This report contains only a small part of the charts and photographs; complete sets may be obtained at the cost of reproduction from the H.S.V.A.

of the step of a float, approximately the same height and breadth at all angles. The spray continues to spread out aft of the planing surface as the trim angle increases. The spray forming at the front edge of the wetted surface flows out laterally in the direction of the bottom of the surface.

Planing surface No. 7 (fig. 20): With medium V-bottom a thin glassy blister of spray proceeds from the contact line of planing surface and homogeneous water(a in fig. 18), and leaves laterally in the direction of the surface as a strong spray at b. The portion marked c indicates the line where the side and the homogeneous water meet. The water here shoots into the air to about the same height and breadth as with the flat surface A, except that the total volume of spray is greater than with surface A, which is explained by the longer, wetted side edge and the larger volume of displaced water. The trough is somewhat longer than for the flat surface A, because the roach retreats toward the rear.

Planing surface No. 8 (fig. 21): The spray on the sides is more extensive than with surface No. 7. The trough maintains for a short distance the depth of the rear edge of the planing surface and follows the shape of the V-bottom.

Planing surface No. 9 (fig. 22): The lateral spray, part of which forms a blister, is of about the same height and breadth as for surface No. 8, next to the rear edge. Aft of the surface, however, it has markedly increased in height and breadth. The deepest point of the trough is at the rear edge of the planing surface.

Planing surface No. 10 (fig. 23): Because of its pronounced angle of V, the mean unit pressure is so reduced that the displaced volume of water at small trim angles is almost equal to the buoyancy (fig. 17), so that in spite of the free edges it is rather a question of floating than of planing. Accordingly, the pressure drop at the sides is small, hence the spray formation is not very extensive. The trough is strongly grooved, and a long, low roach is formed closely aft of the planing surface. After a steady increase in spray formation up to an angle of V lying between 132° and 100°, any subsequent rise in keel angle produces a marked decrease in spray.

STABILITY

If the water is in a disturbed condition the running onto a wave crest momentarily increases the wetted surface, whereby the center of lift is shifted forward. In the next moment the wave trough is passed and the opposite occurs; the wetted surface is momentarily smaller and the center of lift shifts aft. In both cases, equilibrium by a change in draft is reached only in part because of the mass inertia. The resulting displacement of the center of lift about its median position at wave frequency causes a longitudinal oscillation. The displacement of the center of pressure referred to the wetted length of the planing surface at identical disturbance of the water is relatively greater as the wetted length is less, that is, as the angle of dead rise is less. Correspondingly, the longitudinal stability increases with the angle of dead rise as substantiated by observation during the tests. By contrast, the lateral stability decreases. For example, surface No. 10, at high trim angles, was markedly unstable transverse to the direction of motion.

EFFECT OF TRANSVERSE CURVATURE

The desire to keep the heavy spray from V-bottoms down laterally, leads to the use of curvature in the sides of the planing bottom, similar, for instance, to the hollow vees used in building planing boats. The planing bottom forms 11 to 15, selected for comparative tests, are shown in section in figure 24.

Planing surface No. 11 has the same angle of V as planing surface No. 9. Figure 25 shows that the minimum resistance lies some 11½ percent lower than the minimum for surface No. 9. The improvement is obtained in part from the sides of the bottom approaching so nearly flat surfaces in that the lift developed at a more favorable planing number produces a smaller resistance. The rest of the gain is attributable to the reaction from the issuing water, of which the direction of motion is changed in the curvature of the bottom. This increases the lift and the wetted surface and the friction are correspondingly decreased. The ensuing pressure rise in the outside curve is seen in figure 26. The greater pressure drop, compared

to surface No. 9, induced toward the edge is followed by a substantially more forceful breaking up of the water. The intended deflection of the water does not occur; instead, the water shoots up on the side at the same angle as with surface No. 9. Because of the greater breaking up, the spray pattern seems to be even more unfavorable than with No. 9. Nevertheless, the area of the spray is somewhat reduced, caused probably by the reduced side length (compared to No. 9) and the reduced static displacement.

Test Data of Planing Surfaces Nos. 11 to 15

Run No.	α	$\frac{F'}{b^2}$	$\epsilon = \frac{W}{A}$	$\frac{M}{A\,b}$
Surface 11: b = 0.3 m; A = 18 kg; v = 6 m/s				
	deg. min.			
36	3 40	3.540	0.1944	2.150
37	4 8	3.175	0.1816	1.938
38	4 16	3.170	0.1805	1.937
39	5 4	2.275	0.1739	1.500
40	5 29	-	0.1711	1.350
41	5 51	1.791	0.1716	1.205
42	6 37	1.440	0.1683	0.989
43	6 50	1.344	-	0.919
44	7 20	1.228	0.1694	0.825
45	8 10	1.000	0.1745	0.710
46	9 17	0.789	0.1800	0.571
Surface 12: b = 0.3 m; A = 18 kg; v = 6 m/s				
47	3 34	3.530	0.1662	2.262
48	3 42	2.900	0.1623	2.037
49	4 21	2.535	0.1555	1.738
50	4 51	1.964	0.1550	1.446
51	5 9	1.705	0.1540	1.434
52	5 34	1.525	0.1483	1.142
53	5 48	1.320	0.1472	0.994
54	6 22	1.137	0.1440	0.850
55	6 51	0.963	0.1428	0.701
56	7 37	0.757	0.1495	0.569
57	8 32	0.672	0.1573	0.508
58	9 2	0.606	0.1650	0.437

Test Data of Planing Surfaces Nos. 11 to 15 (cont.)

Run No.	α	$\frac{F'}{b^2}$	$\epsilon = \frac{W}{A}$	$\frac{M}{A\ b}$
	Surface 13: b = 0.3 m; A = 18 kg; v = 6 m/s			
	deg. min.			
59	3 17	4.925	0.2182	2.504
60	4 4	3.760	0.1922	2.045
61	4 30	3.100	0.1872	1.748
62	5 12	2.418	0.1800	1.445
63	5 21	2.418	0.1800	1.452
64	6 3	-	0.1734	1.150
65	6 38	1.676	0.1738	1.009
66	7 -	1.488	0.1738	0.859
67	7 21	-	0.1767	0.715
68	8 23	1.021	0.1822	0.583
69	9 22	0.818	0.1966	0.451
70	9 55	-	0.2040	0.408
	Surface 14: b = 0.3 m; A = 18 kg; v = 6 m/s			
71	3 43	4.030	0.1945	2.230
72	4 8	3.025	0.1805	1.778
73	4 25	3.025	0.1811	1.780
74	4 43	3.030	0.1795	1.480
75	5 17	1.980	0.1700	1.180
76	5 52	1.715	0.1690	1.032
77	6 21	1.515	0.1692	0.884
78	7 30	1.082	0.1733	0.666
79	8 29	0.957	0.1778	0.604
80	8 45	-	0.1855	0.536
81	9 25	-	0.1905	0.483
82	9 25	-	0.1916	0.483
83	10 41	-	0.2094	0.427
	Surface 15: b = 0.3 m; A = 18 kg; v = 6 m/s			
84	4 4	3.390	0.2155	1.970
85	4 42	2.630	0.2033	1.520
86	5 16	2.035	0.1845	1.212
87	5 47	1.780	0.1778	1.065
88	6 21	1.590	0.1755	0.916
89	6 42	1.352	0.1783	0.773
90	7 -	1.173	0.1822	0.710
91	7 12	1.053	0.1810	0.670
92	8 23	0.874	0.1945	0.500
93	9 9	0.805	0.2090	-

The purpose of testing surface No. 12 was to establish whether with less dead rise the increase in resistance due to the dead rise, could be nullified with transverse curvature. Figure 25 shows that in part values are reached even less than those for the flat surface A. The spray measurements (fig. 27) show that the forward spray that came from surface No. 7 with the same angle of V is flattened out by the transverse curvature. The spray is not quite so high at and aft of the rear edge of the planing bottom, but is laterally more spread out.

Surfaces Nos. 13 to 15, having the same angle of V, were studied for the effect of different side curvature. The resistance comparison in figure 25 reveals a 2.5 percent lower minimum for No. 14 than for No. 13, which is explained by the increased spray reaction and its effect on wetted surface and frictional resistance. With too much curvature, surface No. 15, the water no longer becomes separated at the edge until at comparatively high angles of trim, as a result of which the additional friction at the sides raises the minimum resistance by 4.6 percent compared to No. 14.

The spray of surface No. 13 (fig. 28) is similar to that of No. 11, but more voluminous aft. Following the sharp vee of the planing bottom, the water in the middle part of the trough flows immediately upward, forming two partial troughs. Compared to No. 13, No. 14 (fig. 29) clearly develops a stronger, higher, and more voluminous spray, due in part to the mutual interference of the streams of water shifted forward before the wetted forward edge. The still more pronounced curve of No. 15 (fig. 30) holds down the lateral spray up to about $\alpha = 15^{\circ}$. At higher trim angles it flows steeply upward. Its height and volume then are less than with Nos. 13 and 14, but in excess of those of surface A. This example shows that an excessive side curvature may delay the appearance of the pure planing condition without in any way being of use.

EFFECT OF LONGITUDINAL CURVATURE

According to the pressure distribution measurement on surface A, the pressure at the forward edge of the wetted surface where the deflection of the water occurs, rises immediately to maximum and rapidly drops again rearward.

If the surface is curved fore and aft the water flowing relatively to the surface undergoes a steady directional change downward, as a result of which the momentum, and correspondingly the pressure, transmitted by the water per unit surface, is greater over the after unit areas than in the case of the flat bottom. This means that the mean pressure on the wetted surface $p_m = A/F'$ increases, and for equal lift F' is reduced, compared to the flat bottom, thus resulting in a gain of frictional resistance W_R at equal angle of trim. In figure 32 the angle of trim α' for the curved surface denotes the setting of the chord corresponding to the wetted length l'.

For comparison with the flat surface A, we investigated surface No. 16, having a radius of curvature $R = 11,500$ mm, and surface No. 17 with $R = 6,000$ mm. These surfaces, 0.3 m width, had a fore-and-aft curve with constant radius, but were flat transversely. Figure 31 shows the minimum resistance of surface No. 16 to be 10.3 percent, and that of surface No. 17, 15.6 percent lower than that of surface A. The decrease in resistance is approximately proportional to the reduction in wetted surface. The moment is reduced to an even greater degree than the wetted surface, because the distance l_p of the resultant from the after edge of the planing surface becomes smaller as the pressure distribution curve becomes fuller. Figure 32, where the ratio l_p/l' versus α is given for the flat and curved surfaces, shows how l_p/l' decreases as the curvature increases.

The spray (figs. 33 and 34) at the sides is substantially less in height and volume compared to the plane surface A, which again is due to the shortened wetted length and to the reduction in static displacement. In contrast with surface A, there is a deeper and wider trough aft of the planing surface. An increasing longitudinal instability is observed with increasing curvature, which is explained in the section "Stability" (page 19), insofar as the curvature is followed by a reduction in wetted length and likewise by an increase in the effect of the displacement of the center of lift in disturbed water.

Test Data of Planing Surfaces Nos. 16 and 17

Run No.	α	$\frac{F'}{b^2}$	$\epsilon = \frac{W}{A}$	$\frac{M}{A\ b}$	$\frac{l_p}{l'}$
	Surface 16:	b = 0.3 m;	A = 18 kg;	v = 6 m/s	
	deg. min.				
94	3 52	2.385	0.1360	1.532	0.639
95	4 24	2.084	0.1322	1.403	0.669
96	5 20	1.535	0.1317	1.102	0.713
97	6 4	0.183	0.1367	0.884	0.741
98	7 11	0.911	0.1490	0.675	0.735
99	8 20	0.700	0.1572	0.542	0.762
100	9 31	0.550	0.1745	0.411	0.733
	Surface 17:	b = 0.3 m;	A = 18 kg;	v = 6 m/s	
101	3 00	2.668	0.1400	1.268	0.472
102	4 6	1.784	0.1266	1.103	0.615
103	4 42	1.468	0.1244	0.967	0.652
104	4 51	1.400	0.1233	0.923	0.655
105	5 28	1.268	0.1266	0.853	0.666
106	6 12	1.017	0.1345	0.713	0.695
107	7 1	0.833	0.1445	0.570	0.677
108	8 36	0.633	0.1655	0.444	0.690
109	9 8	0.544	0.1717	0.379	0.688
110	11 48	0.383	0.2110	0.270	0.685

In conclusion, the following statements may be made as to the spray formation of all the bottom shapes investigated:

1. As the angle of dead rise increases, the spray becomes higher and more voluminous. Not until extremely sharp vees are reached, where the planing rather resembles floating, does the spray formation recede.

2. Transverse curvatures do not have the anticipated effect relative to the restriction of spray. If a reduction occurs, it is minor; in many instances an increase is observed. Excessive transverse curvatures are unfavorable as they are apt to delay the appearance of the pure planing condition. Best of all, is a transition of the side into the horizontal at not too rapid a rate.

3. Longitudinal curvatures, in the case of the transversely flat surfaces reported here, give a favorable spray pattern.

4. The spray is only slightly affected by the form of the planing bottom. It is much more affected by variations in the width of the planing bottom, regarding which there will be a report later.

The comparison of the resistances of all the bottom shapes refers to the condition of pure planing. The mutual interdependence that has been found is qualitatively the same for load changes, and quantitatively about the same according to the results of tests with the flat planing surface A, as described in reference 1. But it does not cover the condition at the change from floating to planing near which the resistance of a seaplane during take-off is a minimum. It remains for special investigation to show whether V'd forms are comparatively superior to flat bottoms at the maximum resistance, which would involve another factor in the compromise solution that must be found in the design of a seaworthy airplane.

The bottom forms described here represent only a fraction of those tested. The results of the tests with other bottom forms will be published later.

Translation by J. Vanier,
National Advisory Committee
for Aeronautics.

REFERENCES

1. Sottorf, W.: Experiments with planing surfaces. T.M. No. 661, N.A.C.A., 1932.

2. Wagner, Herbert: Landing of Seaplanes. T.M. No. 622, N.A.C.A., 1931.

3. Pabst, Wilhelm: Landing Impact of Seaplanes. T.M. No. 624, N.A.C.A., 1931.

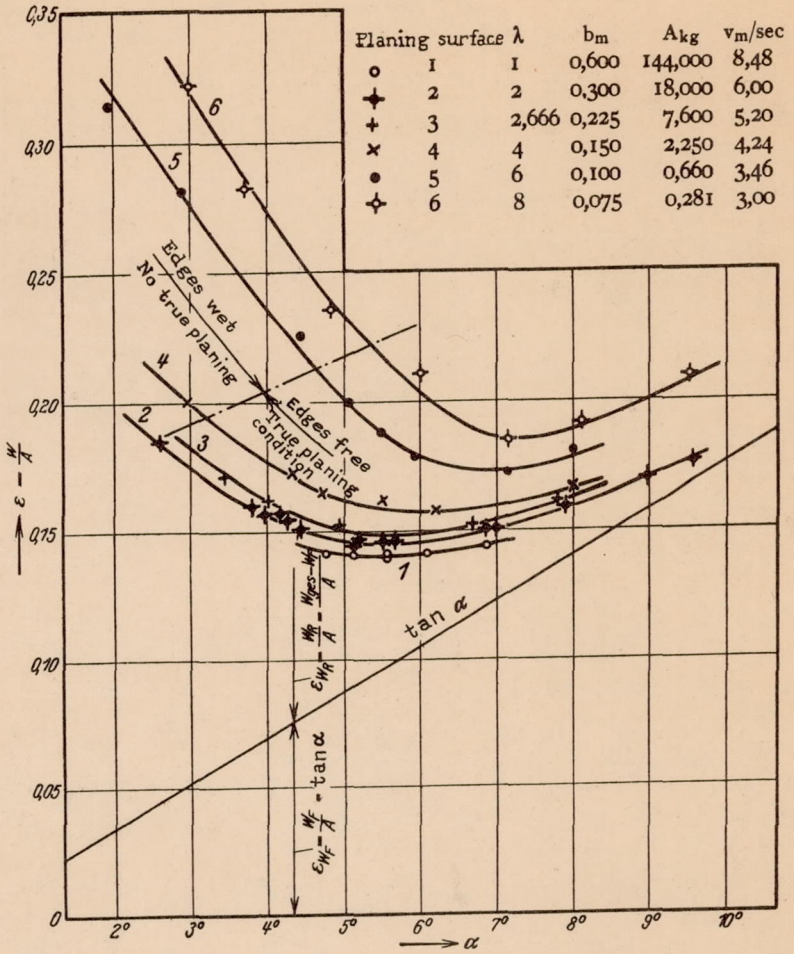

Figure 1.- Planing number ε versus α for flat planing surfaces towed according to Froude law.

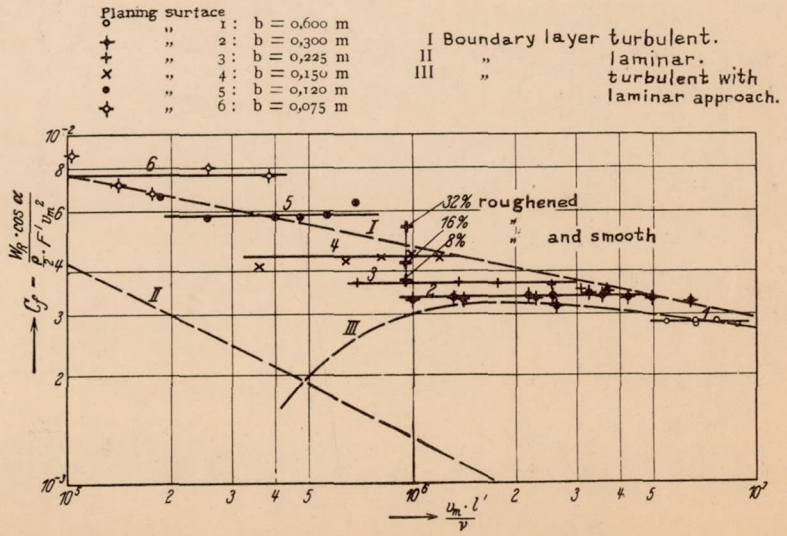

Figure 2.- Coefficient of friction versus Reynolds Number for flat planing surfaces.

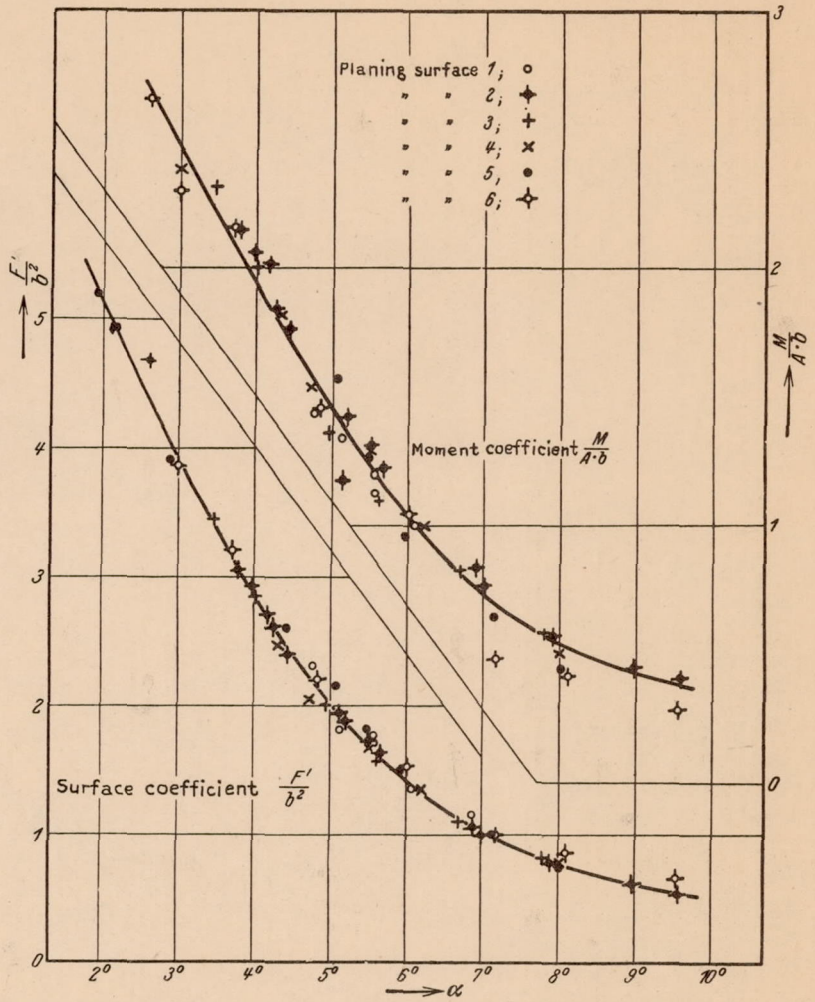

Figure 3.- Coefficients of surface F'/b^2 and moment M/Ab versus α.

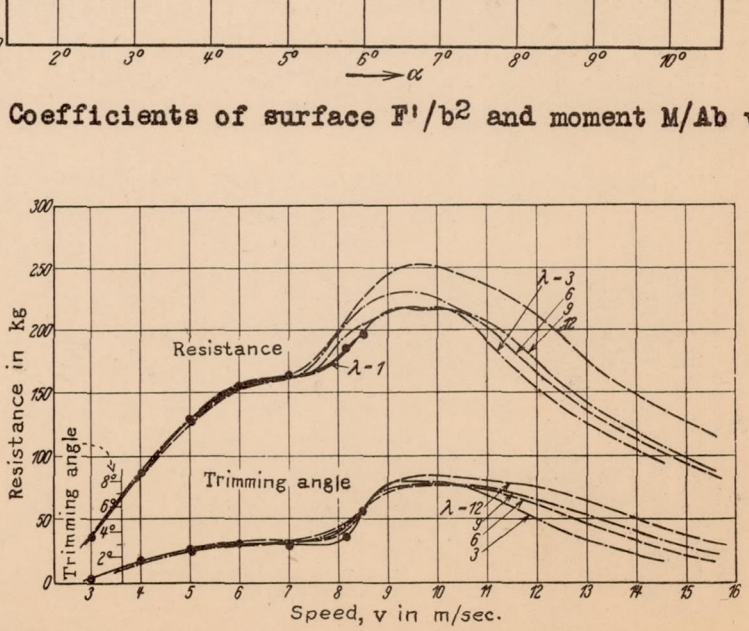

Figure 4.- Resistance and angle of trim, full size, for M_1 = const. together with resistance and trim angle converted according to λ^3 for scale $\lambda = 3, 6, 9$ and 12 at the same moment.

Figure 5.- Resistance and angle of trim, full size, for M_2 = const. together with resistance and trim angle converted according to λ^3 for scale λ = 3,6,9 and 12 at the same moment.
(Right) Resistance of the models at the same trim angle as for full size.

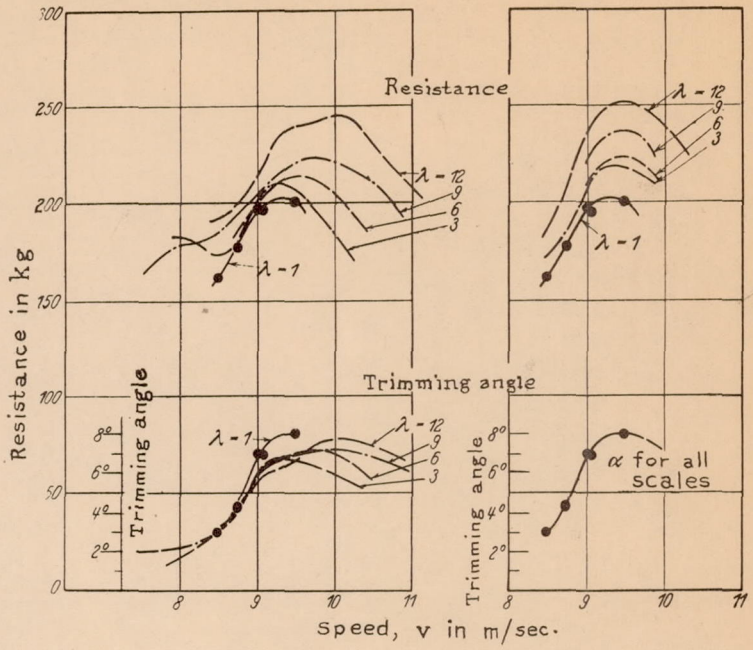

Figure 6.- Percent increase of hump resistance versus scale.

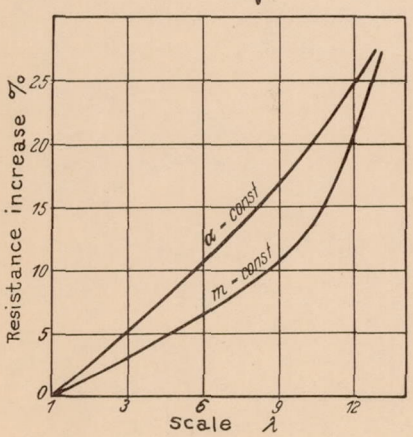

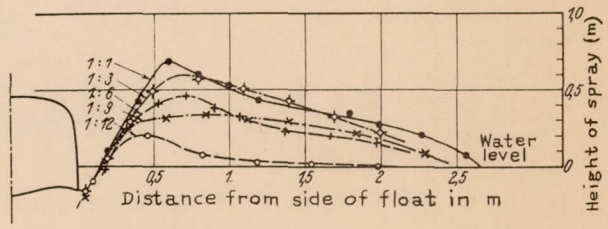

Figure 7.- Spray formation, measured at full-scale transversely 500 mm forward of step at v = 8.75 m/sec. and on all models at similar distance and corresponding speeds, reduced to 1 : 1.

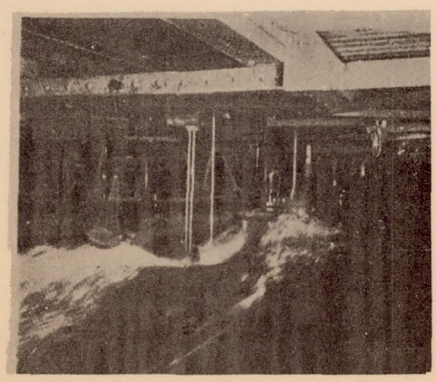

Fig. 8.
$\lambda = 3$, $\alpha = 6°$, $v = 5{,}5$ m/s with $V = 9{,}5$ m/s.

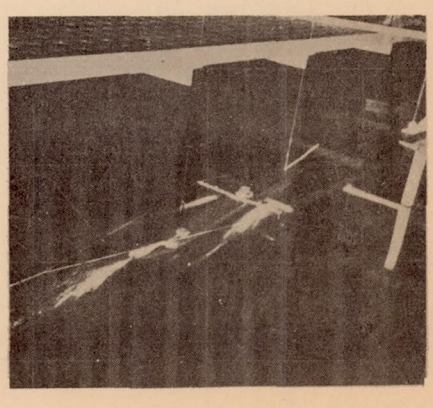

Fig. 9.
$\lambda = 12$, $\alpha = 6°$, $v = 2{,}75$ m/s with $V = 9{,}5$ m/s.

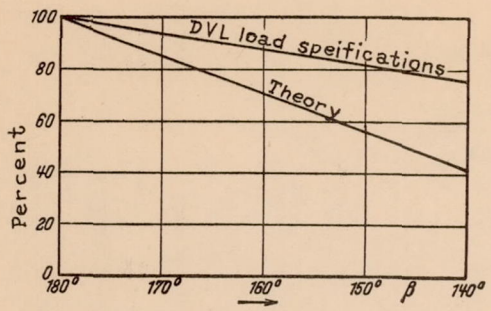

Figure 10.- Effect of keel angle β on impact.

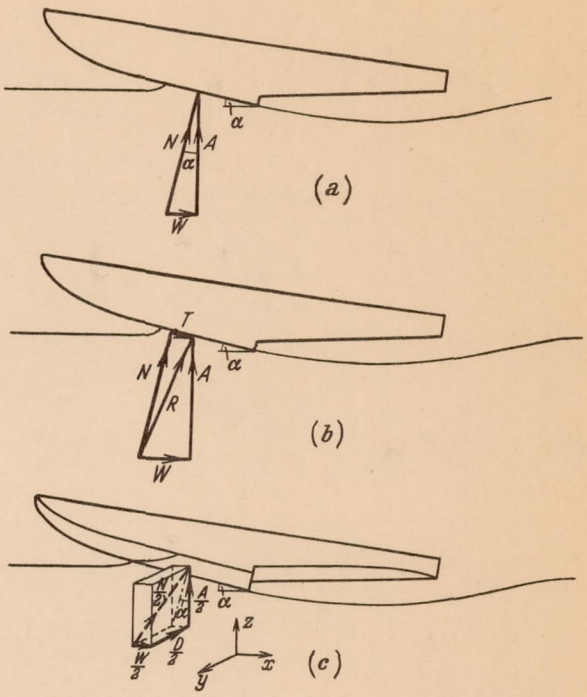

Figure 11.-
(a) forces on flat float bottom, frictionless fluid,
(b) " " " " " , viscous " ,
(c) " " V " " , frictionless " .

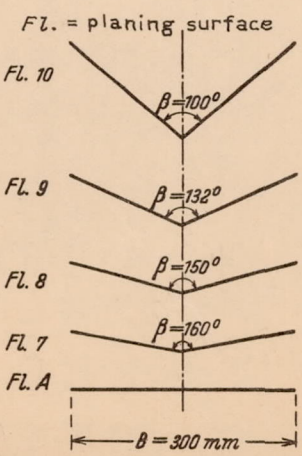

Figure 12.- Sections of planing surfaces A and nos. 7-10.

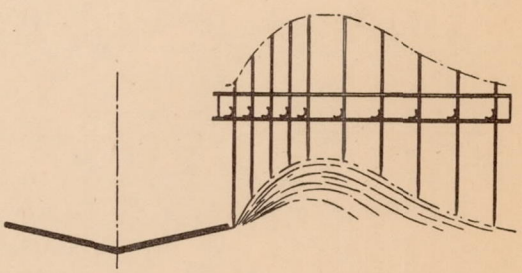

Figure 13.- Device for measuring spray.

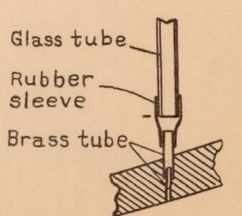

Figure 14.- Pressure recording orifice.

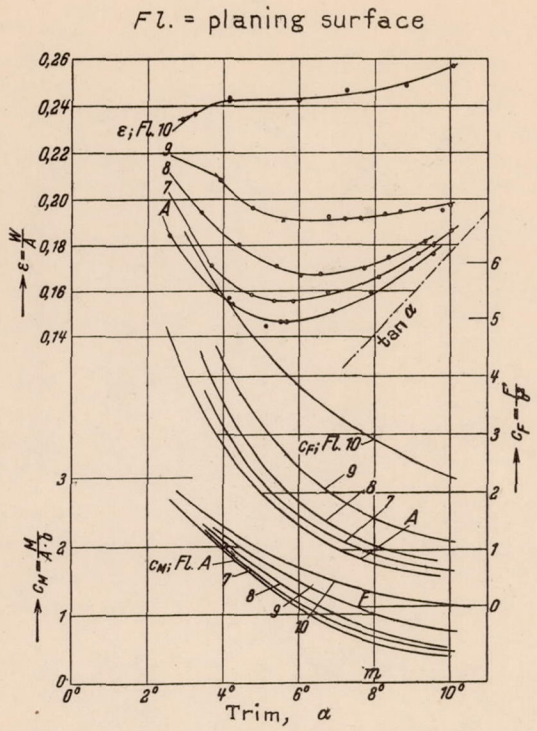

Figure 15.- ϵ, c_M and c_F versus α for surfaces A, and nos. 7-10.

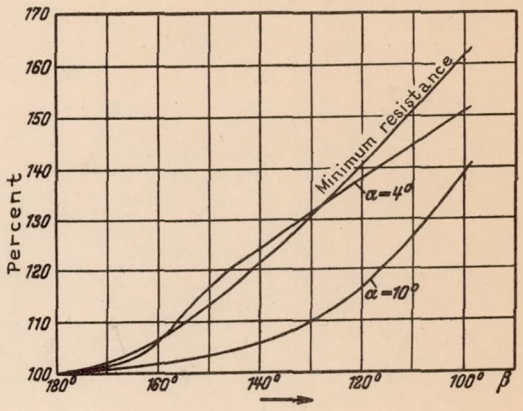

Figure 16.- Effect of keel angle β on resistance at $\alpha = 4^\circ$, 10°, and at minimum resistance.

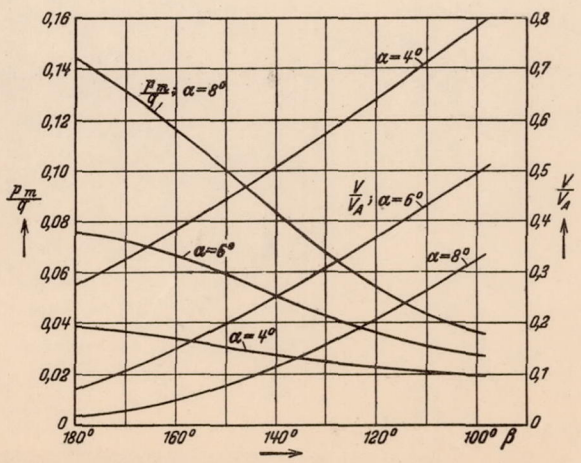

Figure 17.- pm/q and V/V_A versus β for $\alpha = 4^\circ$, 6° and 8°.

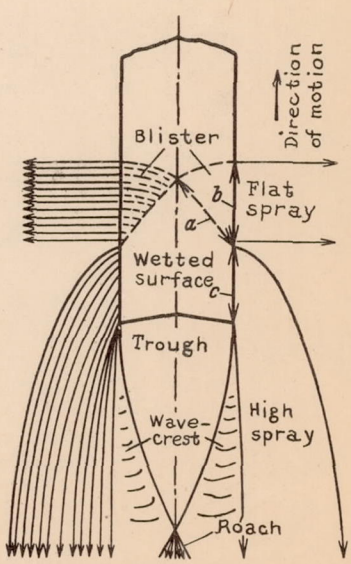

Figure 18.- Top view of spray of V-float.

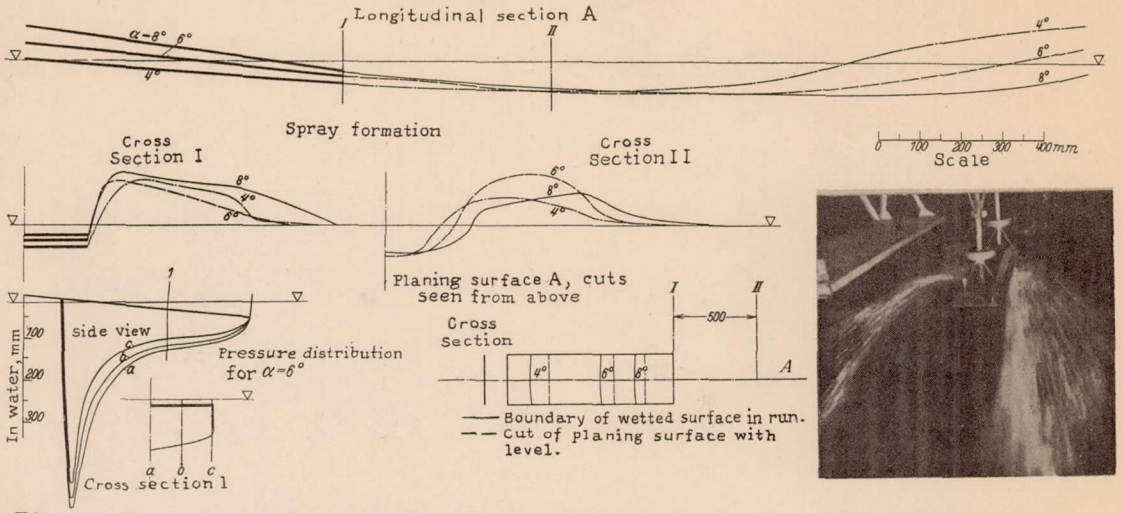

Figure 19.- Spray formation and pressure distribution of surface A at 6 m/sec. speed and 18 kg load.

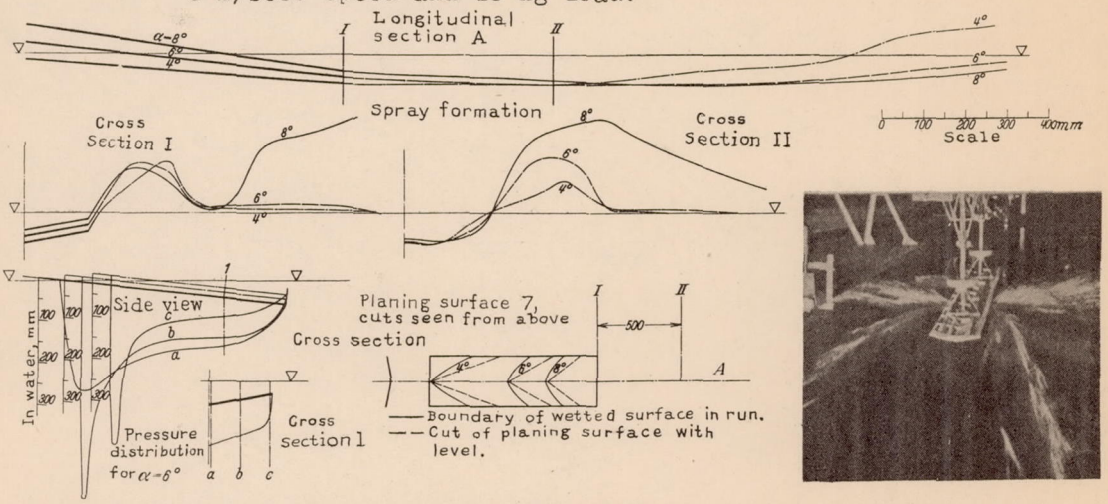

Figure 20.- Spray formation and pressure distribution of surface no.7 at 6 m/sec. speed and 18 kg load.

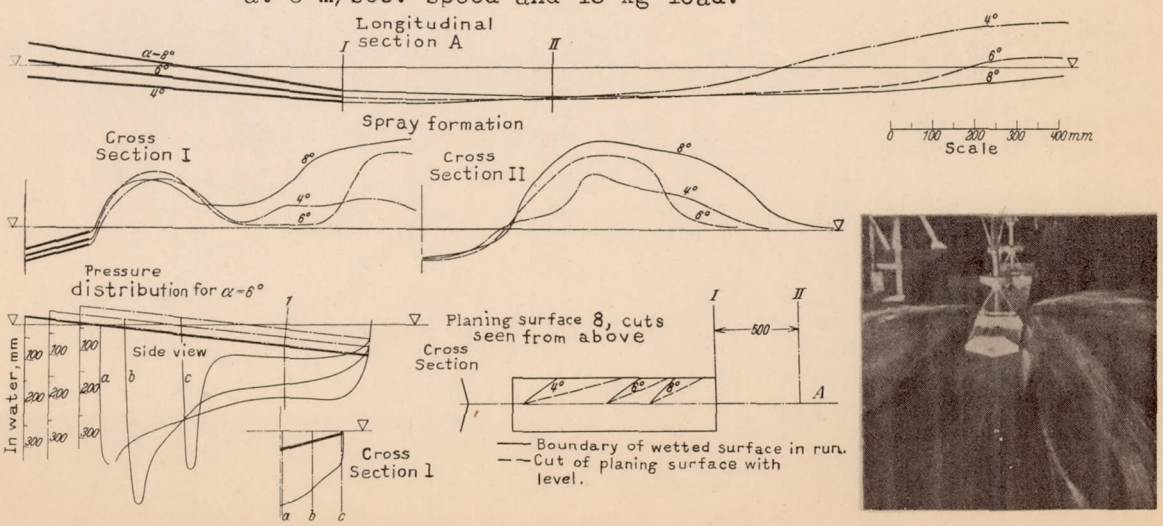

Figure 21.- Spray formation and pressure distribution of surface no.8 at 6 m/sec. speed and 18 kg load.

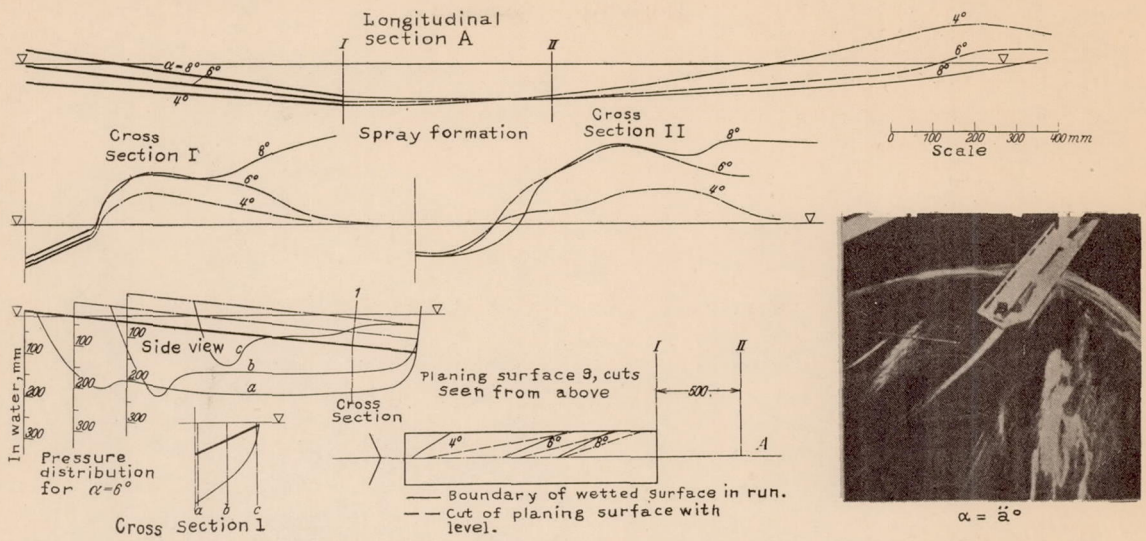

Figure 22.- Spray formation and pressure distribution of surface no.9 at 6 m/sec. speed and 18 kg load.

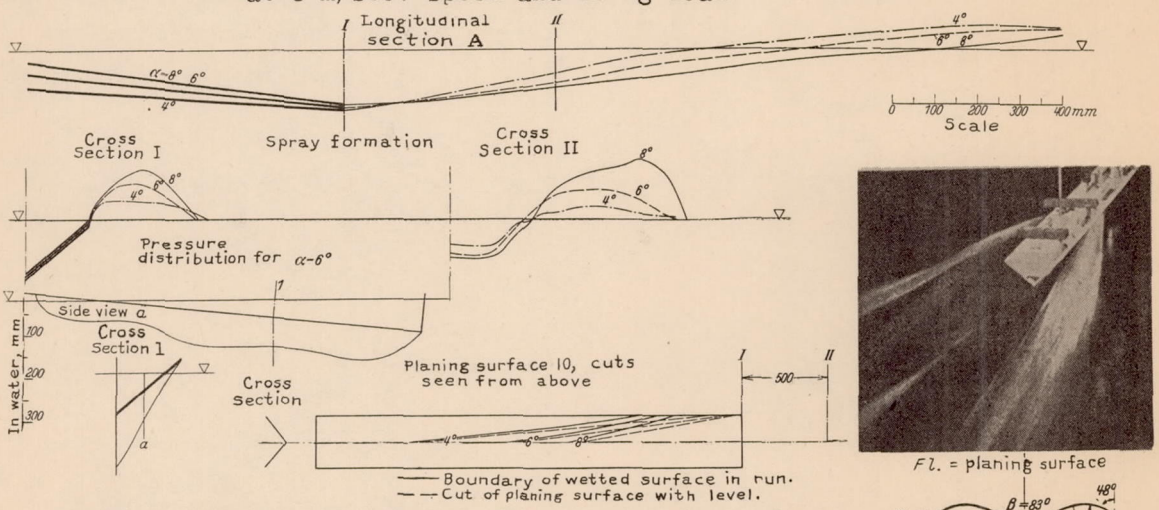

Figure 23.- Spray formation and pressure distribution of surface no.10 at 6 m/sec. speed and 18 kg load.

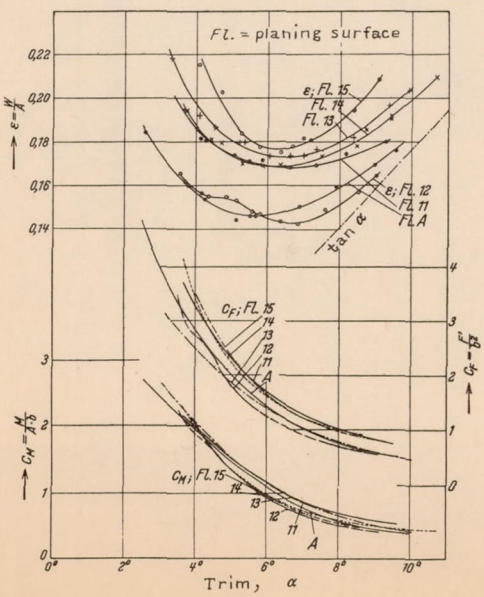

Figure 24.- Cross section of planing surface no.11-15.

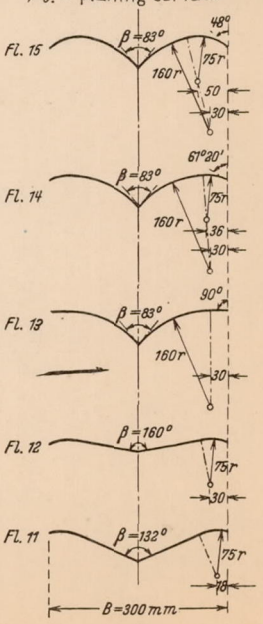

Figure 25.- ϵ, c_M and c_F versus α for A, and no.11-15.

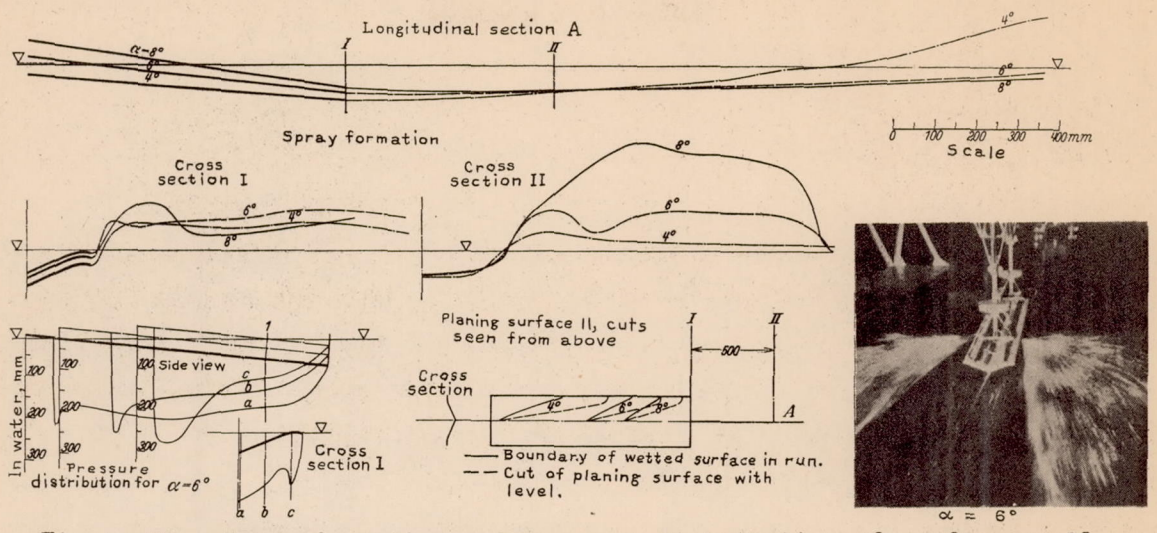

Figure 26.- Spray formation and pressure distribution of surface no.11 at 6 m/sec. and 18 kg load.

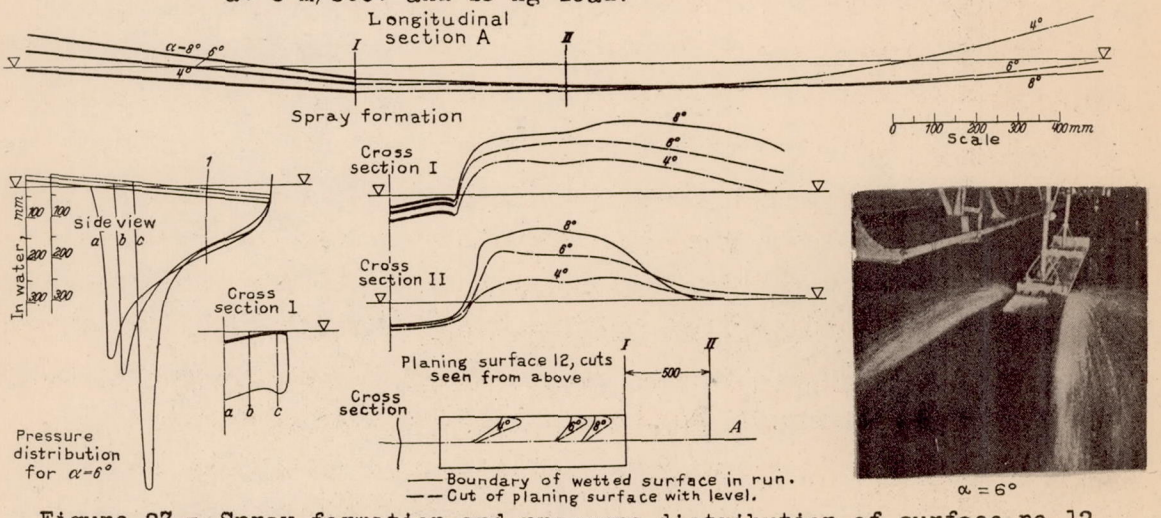

Figure 27.- Spray formation and pressure distribution of surface no.12 at 6 m/sec. and 18 kg load.

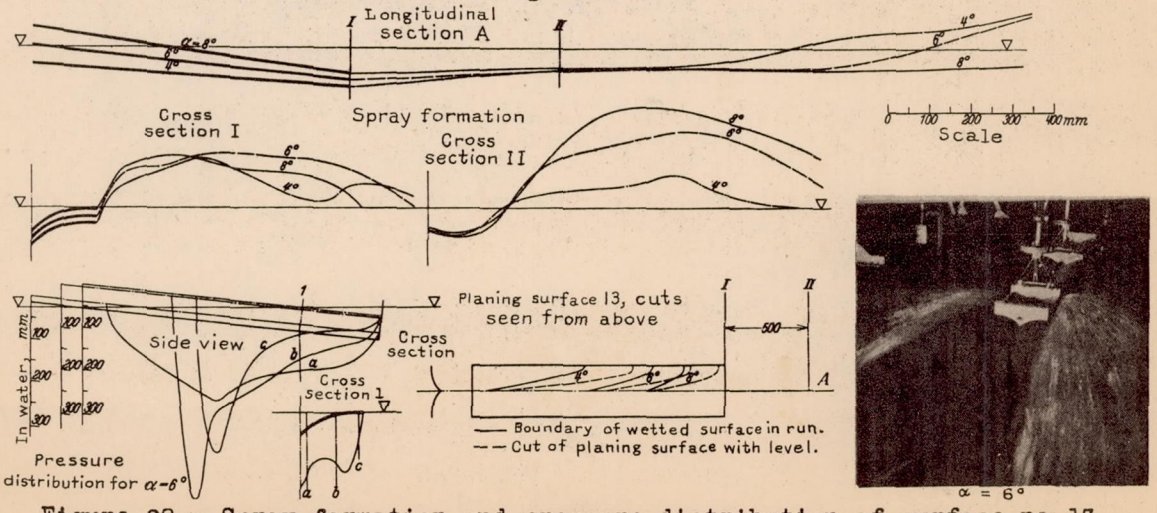

Figure 28.- Spray formation and pressure distribution of surface no.13 at 6 m/sec. and 18 kg load.

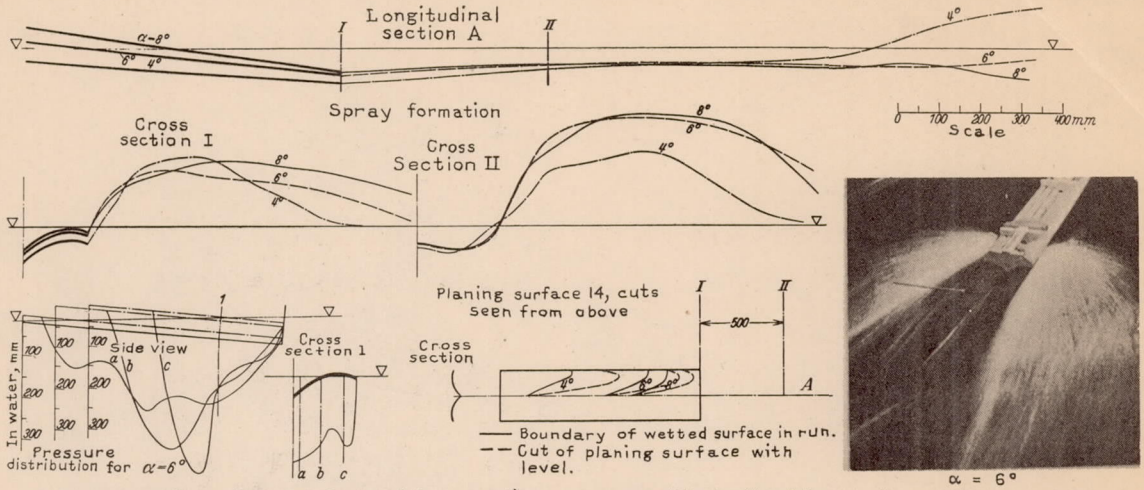

Figure 29.- Spray formation and pressure distribution of surface no.14 at 6 m/sec. and 18 kg load.

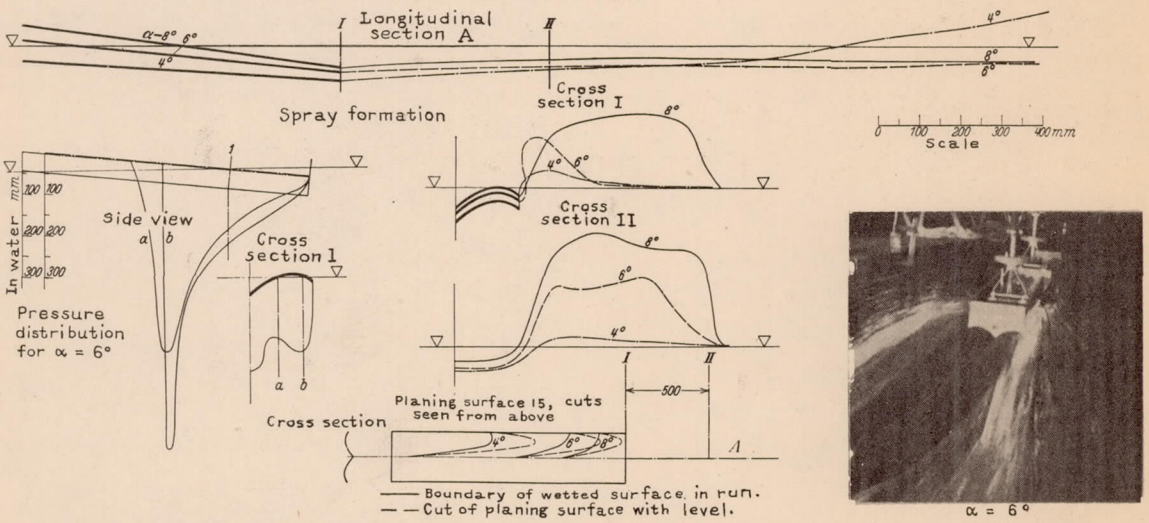

Figure 30.- Spray formation and pressure distribution of surface no.15 at 6 m/sec. and 18 kg load.

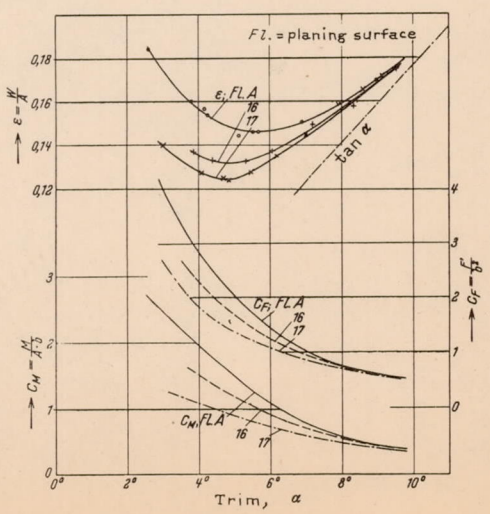

Figure 31.- ε, c_M and c_F versus α for surface A, and 16-17.

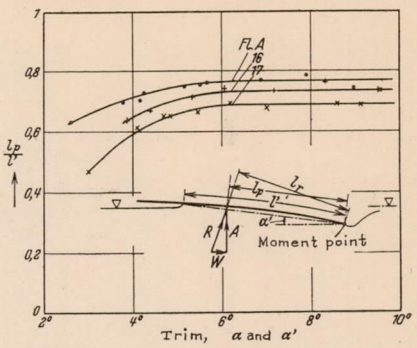

Figure 32.- l_p/l' versus α for surface A, and 16-17.

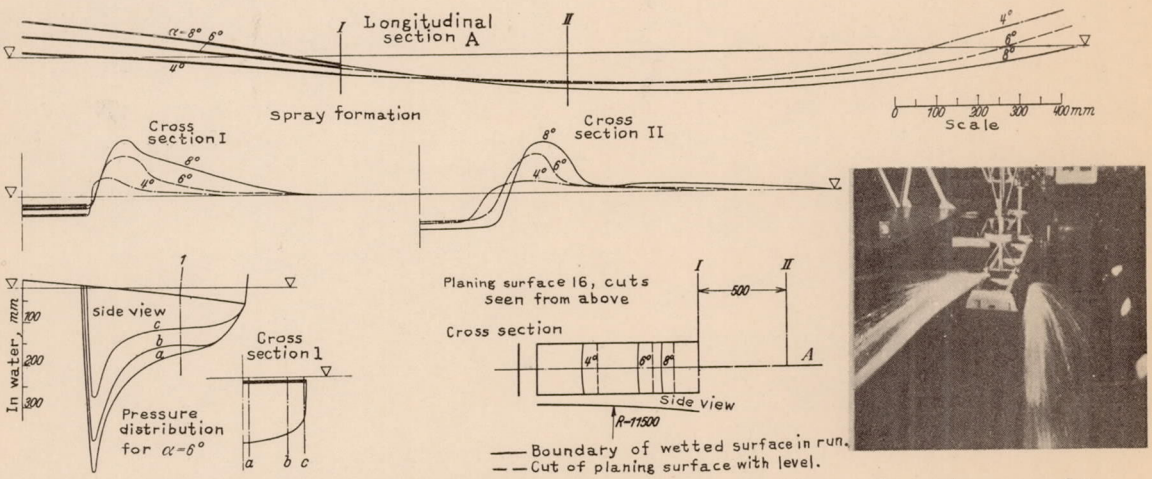

Figure 33.- Spray formation and pressure distribution of surface no.16 at 6 m/sec. and 18 kg load.

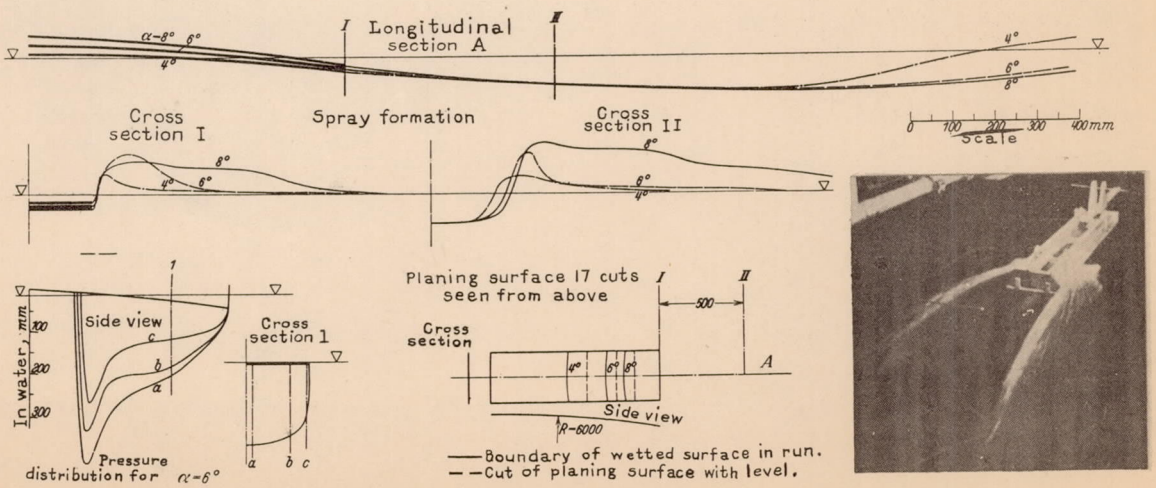

Figure 34.- Spray formation and pressure distribution of surface no.17 at 6 m/sec. and 18 kg load.